Sliding friction dynamics of hard single asperities on soft substrates

Sliding friction dynamics of hard single asperities on soft substrates

W. P. Vellinga[1,*] and C. P. Hendriks[2]
[1]*Materials Technology, Mechanical Engineering, Eindhoven University of Technology, P.O. Box 513, 5600 MB Eindhoven, The Netherlands*
[2]*Philips Centre for Industrial Technology (CFT), P.O. Box 218, 5600 MD Eindhoven, The Netherlands*
(Received 8 November 2000; published 24 May 2001)

The sliding friction of hard, micron-sized single asperities sliding on soft polyester films was studied. Transitions from steady sliding to so-called ''stick-slip'' or nonstationary motion occur for decreasing driving speed, decreasing driving spring stiffness, increasing normal load, decreasing tip radius, and decreasing crosslink density. Normal displacements of the tip during sliding were studied in some detail. It is argued these play an important role in the dynamics of the system, being the dominant factor in determining the contact area between asperity and substrate. A rather simple model is proposed that is related to rate-and-state descriptions of stick-slip phenomena. In this particular description the normal displacement plays a part analogous to that of the state parameter. In a limited comparison of experiment and numerical results we find qualitative agreement on all measured trends.

DOI: 10.1103/PhysRevE.63.066121 PACS number(s): 81.40.Pq, 46.55.+d

I. INTRODUCTION

Scientific research into sliding friction aims to identify and quantify physical mechanisms that lead to dissipation in sliding contacts. In the last decade or so, two modifications of the previous experimental situations have proven to be very important:

(1) the use of ''single asperity'' contacts,

(2) delibirate study of dynamic sliding behavior of sliding contacts by excursions in the dynamical parameter space.

A sketch of a typical experimental situation is shown in Fig. 1. Single asperity contacts can be much better defined than everyday multiple asperity contacts, which allows one to critically compare theory and experiment. Well-established single asperity techniques are friction force microscopy (FFM) [1] and the Surface Force Apparatus (SFA) [2]. Recently we have described an apparatus, the lateral force apparatus (LFA) [3], Fig. 2, that allows single asperity measurements in a different range of contact situations [Fig. 4(a)–4(b), also Secs. II E and II F].

Studies of *friction dynamics* have attracted a considerable amount of attention in recent years. A typical sliding friction experiment, Figs. 3(a)-3(g), starts at some time $t=0$ when the asperity is brought into contact with the surface with normal force F_n and at position $x=0$. The driving equipment starts moving the base of a cantilever with lateral stiffness k_l at time $t=t_0$, and quickly reaches v_s. The extension of the spring is measured during some time, which leads to a time series of lateral force values $F_l(t)=k_l[v_s t-x(t)]$. The behavior of $F_l(t)$ in time is found to depend both on the properties of the loading equipment and on the physical properties of the contact. If the properties of the loading equipment are known, hypotheses on the physical behavior can lead to predicted time series of $F_l(t)$ that can be compared to experiments. To focus on these physical mechanisms it has proven essential to have an experimental record that spans a wide region in dynamic parameter (i.e., t_0, v_s, k_l, F_n) space (Fig. 1 and Fig. 3, Sec. II A). Interestingly, dynamic behavior encountered in sliding systems operating at widely different lengthscales and in seemingly very different physical circumstances, shows many common characteristics. Examples of such similar behavior occur in earthquakes [4–6], confined layers of fluids (boundary lubrication) [7], granular materials [8–10], and paper-paper contacts [11,12].

A combination of these two developments, that is the study of friction dynamics of single asperities, has proven to be very fruitful in the field of boundary lubrication, partly due to the possibility of comparison with molecular-dynamics calculations [13]. In contrast the studies on ''dry'' friction dynamics, friction between unlubricated solids (Sec. II), have all been performed on multiasperity systems. Studies of single asperity dry friction dynamics, such as described in this paper, are therefore an interesting way to proceed.

The system studied consists of hard, rigid, asperities sliding on, or ploughing through, soft polyester layers. And indeed key aspects of the friction dynamics observed in other systems, are also present in the experiments reported here (Sec. III B). We anticipate that the observed behavior is relevant for the friction and wear behavior of many polymers and polymer coated metals.

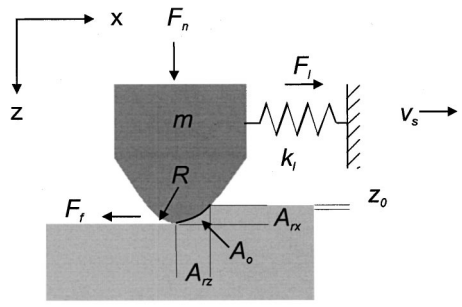

FIG. 1. Sketch of a single asperity sliding contact. The dynamical parameters used in the text are shown in the figure.

*Email address: willem@wfw.wtb.tue.nl

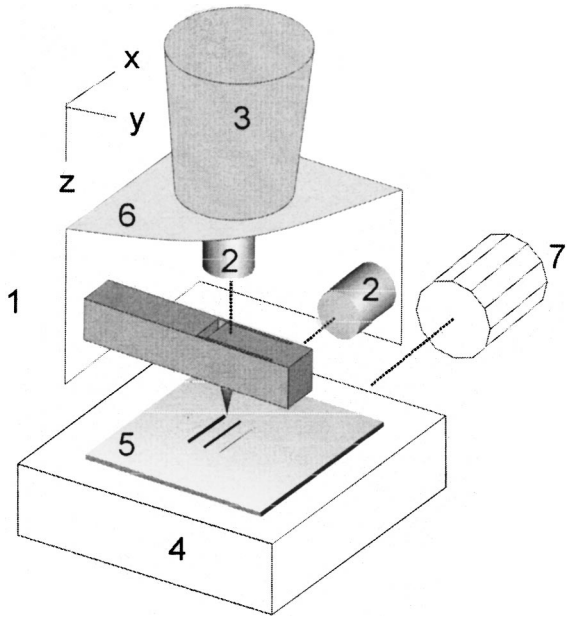

FIG. 2. Sketch of the experimental apparatus, LFA (1) leaf-spring unit, (2) optical focus error heads, (3) piezoelement in feedback-loop, (4) sample stage, (5) sample, (6) frame, and (7) motor for sample movement. (For more detailed explanation see Sec. III A.)

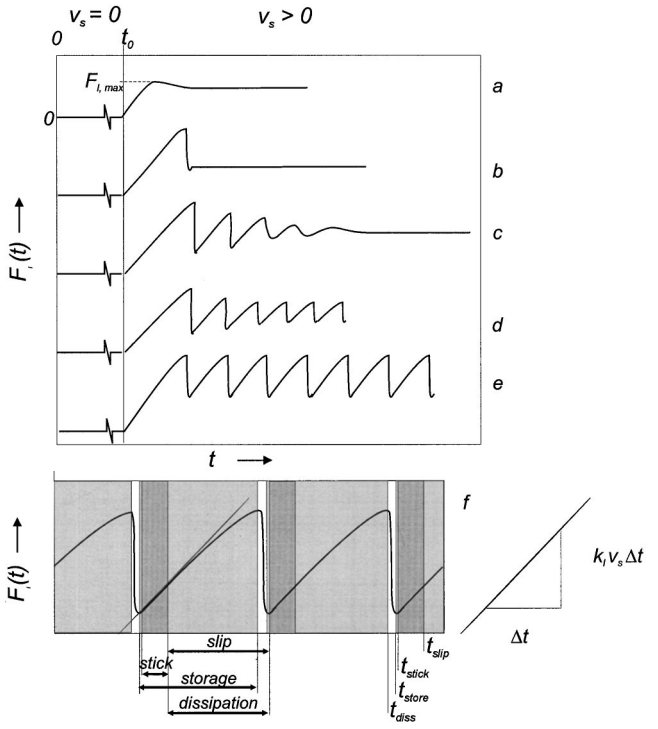

FIG. 3. Sketch of typical measurements encountered in sliding friction experiments. (a)–(c). Steady sliding with differing transitory behavior. (d)–(e). Stick-slip behavior with differing transitory behavior. Note differing values of $F_{l,\max}(f)$: Stick-slip behavior. Relevant times and time periods discussed in the text are indicated. The terms ''storage'' and ''dissipation'' refer to energy of the driving spring.

Based on the experimental record we propose a rather simplified physical description of the experiment that nevertheless leads to useful insight in the complexity of the dynamics, (Sec. IV A). This description is compared to the well-established rate-and-state formulations that have been successful in capturing the phenomenology of friction dynamics. The descriptions are shown to be analogous. However, in the description presented here, the usual phenomenological state parameters are absent. Instead others appear that are more clearly related to measurable quantities and to descriptions of the behavior of the substrate material in terms of constitutive relations. All experimentally observed trends are qualitatively reproduced (Secs. IV B, IV E).

The paper is organized as follows: relevant background will be discussed first, in Sec. II. The aim is to make clear where this paper fits in already existing experimental and conceptual framework and where new elements are introduced. The experimental set up and results are presented in Sec. III. A model description of the experiments is given in Sec. IV. Discussion and conclusions follow in Secs. V and VI.

II. BACKGROUND

A. Dynamic sliding friction

Sketches of typical time series of experimentally observed dynamic behavior during this and other work on dynamic friction are shown in Fig. 3. Transitory behavior eventually gives way to steady sliding $(a-c)$ or stick slip (d and e). The transitory behavior depends on t_0, the time between application of the load F_n at $t=0$, and the start of the driving of the spring, with stiffness k_l. This is, for example, apparent in the different maximum values $F_{t,\max}$ of $F_l(t)$ in the time series a, b, and c. The steady-state dynamic behavior is sensitive to the dynamic parameters; for certain parameters, usually for lower v_s, lower k_l, and higher F_n, ''stick-slip'' appears. The following balance of forces must exist in the sliding direction:

$$m\ddot{x}(t)=k_l[v_s t-x(t)]-F_f(t)\Rightarrow m\ddot{x}(t)=F_l(t)-F_f(t), \tag{1}$$

where m is the mass of the probe, and $F_f(t)$ the friction force exerted by the substrate on the asperity. Whenever $\ddot{x}(t)=0\Rightarrow F_l(t)=F_f(t)$.

One often encounters a strict qualitative distinction between ''static'' and ''kinetic'' friction. A static friction force $F_{f,\text{static}}$ is defined as the highest value that $F_l(t)$ reaches before sliding sets in. (Although, in in practice, it is more often applied to $F_{l,\max}$ at which time $\dot{x}$ equals v_s, and not zero, see below.) ''Kinetic friction,'' $F_{f,\text{kinetic}}$ is defined as the friction force during sliding and often taken to be a simple function of the driving speed v_s; $F_{f,\text{kinetic}}=F_{f,\text{kinetic}}(v_s)$. However, it is impossible to describe the behavior shown in Fig. 3 using these assumptions in Eq. (1). Furthermore because the movement gradually evolves from a stick-slip-like character to a steady sliding character, it appears that there may be no need to invoke qualitative differences between the sliding contact in those cases. Qualitatively different sliding behavior does

not necessarily mean that different physical mechanisms are at work. In fact rather simple sets of coupled nonlinear ordinary differential equations may show behavior of the dependent variables that is very similar to that shown in Fig. 3. In the terminology of such systems stick slip would be an instance of a ''relaxation oscillation,'' an oscillatory process with widely differing time scales within one period [14].

It is useful to define exactly what is meant by stick slip. In fact stick-slip-like movements in sliding friction are more generally characterized by alternating periods of energy storage and periods of energy dissipation in the driving spring. For all t

$$P_{\mathrm{tot}}(t)=F_l(t)v_s=P_{\mathrm{sto}}(t)+P_{\mathrm{diss}}(t). \tag{2}$$

Here $P_{\mathrm{diss}}(t)$ refers to all power that is not stored in the driving spring and that is somehow converted, e.g., to heat or to an increase of the free energy of the substrate. The following holds:

$$P_{\mathrm{sto}}(t)=F_l(t)[v_s-\dot{x}_{\mathrm{tip}}(t)] \quad \text{so} \quad P_{\mathrm{diss}}(t)=F_l(t)\dot{x}_{\mathrm{tip}}(t). \tag{3}$$

The two extreme cases are steady sliding $P_{\mathrm{sto}}=0$, and stick $P_{\mathrm{diss}}=0$. During steady sliding $P_{\mathrm{diss}}(t)=F_l(t)v_s$, and during stick $P_{\mathrm{sto}}(t)=F_l(t)v_s$. Of course $\dot{x}_{\mathrm{tip}}(t)$ must be continuous for all t. If stick occurs, it follows that at some later time $t=t_{\mathrm{slip}}, d^2F_l/dt^2<0$. t_{slip} is the actual time of transition from stick to slip, see Fig. 3(f). t_{slip} also coincides with the time at which dissipation starts, $P_{\mathrm{diss}}>0$, and some of the power transferred to the system by the driving apparatus is now dissipated in the substrate. However, storage in the spring continues until at some $t=t_{\mathrm{diss}}$. $dF_l/dt=0$ or $\dot{x}=v_s$. After t_{diss} only dissipation occurs until at some $t=t_{\mathrm{store}}$ storage starts again. Dissipation stops whenever $d^2F_l/dt^2=0$ at some $t=t_{\mathrm{stick}}$. Between t_{stick} and t_{slip} only storage occurs. Measuring t_{slip} is problematic for a number of reasons. First of all, drift and noise limit the smallest value of velocity that can reliably be measured. Uncertainties in driving speed and spring stiffness, as well as in substrate compliance, add complications in ruling out that the tip is in fact moving at an extremely low speed with respect to the surface. This means, that in practice, it is hard to judge whether t_{stick} and t_{slip} actually exist.

B. Rate-and-state formulations

A key realization has been that qualitatively very different sliding behavior, such as shown in Fig. 3, within a certain sliding system, does not *necessarily* mean that qualitatively different physical mechanisms are at play. This realization is at the heart of the rate-and-state descriptions [6,7] that have the following general form:

$$m\ddot{x}(t)=k_l[v_st-x(t)]-F_f(t) \quad \text{with}$$

$$F_f=F_f(\dot{x},\vartheta_1,\ldots,\vartheta_n), \quad \dot{\vartheta}_i=\vartheta_i(\dot{x},\vartheta_1,\ldots,\vartheta_n) \quad \text{and}$$

$$\dot{\vartheta}_i=\vartheta_i(\dot{x},\vartheta_1,\ldots,\vartheta_n). \tag{4}$$

In general this is a system of coupled nonlinear ordinary differential equations, quite capable of showing relaxation oscillations for certain parameter combinations.

These descriptions contain one or more ''state'' parameters ϑ_i with ''evolution laws'' $\dot{\vartheta}_i(\dot{x},\vartheta_l,\ldots,\vartheta_n)$. The state parameters *and* their evolution laws are usually largely phenomenological and chosen to reproduce or fit the experimental record of dynamic behavior. In this respect they can be rather adequate [11]. In some well-known formulations, relevant to the situation discussed here, only one state parameter ϑ is used and the difference between the descriptions appear only in the assumed governing equations.

The state parameters ϑ_i and their evolution laws cannot be expected to relate to the same physical process in all systems mentioned in the Introduction. Providing rate-and-state formulations with a physical background is therefore interesting. It is also of practical importance because it is obviously related to eventual predictive capabilities.

In rate-and-state models of ''dry'' friction (Sec. II F) systems the single state parameter ϑ is associated with the ''real'' contact surface A_0 evolving in time. This view is adopted here (Secs. II D and II F) and it is proposed, based on experimental evidence (Sec. III B) that a useful relation exists between the z position of the rigid asperity (Fig. 1) and A_0 for all t (Secs. III, and IV A). Measuring z therefore provides information on the evolution of the state parameter A_0 or alternatively z itself can be viewed as a state parameter.

C. Forms for F_f or friction ''laws''

Experimental results on friction have long been discussed in terms of the purely phenomenological Amontons-Coulomb ''law.''

$$F_f=\mu F_n, \tag{5}$$

with μ the ''friction coefficient.'' A more basic relation is expected to read

$$F_f=\tau A_{rz}, \tag{6}$$

with τ some stress or modulus related to the slip process, and A_{rz} the contact surface projected along the surface normal. Equation (5) is often expanded to account for an adhesion force $F_{\mathrm{adh}}=p_{\mathrm{adh}}A_{rz}$, with p_{adh} the adhesive pressure

$$F_f=\mu(F_{\mathrm{adh}}+F_n). \tag{7}$$

Equation (6) is often expanded assuming a linear dependence of τ on pressure: $\tau=\tau_0+\alpha p_m$ with $p_m=F_n/A_{rz}$:

$$F_f=(\tau_0+\alpha p_m)A_{rz}. \tag{8}$$

Note that Eqs. (7) and (8) are both of the form

$$F_f=C_1A_{rz}+C_2F_n, \tag{9}$$

with c_1 and c_2 some constants. The work of Greenwood and Williamson explained that F_n and A_{rz} are proportional for certain multiasperity interfaces, in which case Eq. (5) and Eq. (6) are equivalent [16]. This does not explain why F_f should be proportional to either A_{rz} or F_n. The fact that for

multiasperity interfaces A_{rz} is proportional to F_n, makes them rather unsuitable probes to answer the question whether Eqs. (5) or (6) is actually at work. This indicates one reason to perform experiments with *single* asperities.

D. Single asperity contacts

A single asperity contact is usually (implicitly) defined as a contact for which $A_0 = A_{rz}$. In a continuum picture, nonadhering elastic isotropic single asperity contacts are called Hertz contacts. Sneddon has listed many useful results on such contacts [17]. For a paraboloid asperity ($\beta x^n = z$ with $n=2$ and $\beta = 1/2R$) in contact with a flat surface one finds

$$A_{rz} = \pi \left(\frac{3F_n R}{4E^*} \right)^{2/3} \quad \text{and} \quad z = \pi R^{1/3} \left(\frac{3F_n}{4E^*} \right)^{2/3} \tag{10}$$

with $E^* = [(1-v_1^2)/E_1 + (1-v_2^2)/E_2]^{-1}$ the reduced modulus, E_i the Young's moduli, and v_i the Poisson's ratios. z is the penetration depth of the asperity in the surface. In this case A_{rz} scales with $F_n^{2/3}$. For strongly adhering surfaces, compliant materials, and large asperity radii, the contact situation is described by the Johnson-Kendall-Roberts (JKR) theory [18]. The contact for stiff materials, weak adhesion, and small asperity radius is described by the Derjaguin-Müller-Toporov (DMT) regime [19] and in it's limits by the Bradley regime. Situations in between have been treated by Maugis [20]. Simple fits that connect all regimes have been put forward recently [21]. All these theories allow calculation of A_{rz} as a function of F_n in the *elastic* regime. In an elastic contact the values of two nondimensional parameters

$$\mu = \left(\frac{Rw^2}{E^* r_0^3} \right)^{1/3} \quad \text{and} \quad p_m = \frac{F_n}{\pi w R} \tag{11}$$

(with in the work of adhesion and r_0 the range of the interaction potential) are useful to assess which contact regime is prevalent [22]. An important realization contained in Eq. (11) is that already for elastic contacts, apart from moduli and interaction potentials, the geometry R, and normal force F_n are important in determining the contact situation of loaded single asperities.

Of course for high enough $p_{\max}$ the contact is no longer elastic and all descriptions mentioned must fail. Their application to viscoelastic contact situations is an active field of research [23]. For deformation of a rigid perfectly plastic flat substrate beneath a rigid asperity of radius R, one finds

$$A_{rz} \approx 2\pi R z \propto F_n/\sigma_0, \quad z \propto F_n/2\pi R \sigma_0, \quad A_{rx} \approx \frac{4\sqrt{2R}}{3} z^{3/2} \tag{12}$$

with σ_0 a yield stress [24]. So in this case A_{rz} is proportional to the load F_n already for single asperities. Another useful relation is that for the value of F_n and the depth z_0 at which the yield stress is reached. One finds:

$$z_0 = \frac{1}{2} \frac{\pi^2 \sigma_0^2 R}{4E^{*2}}. \tag{13}$$

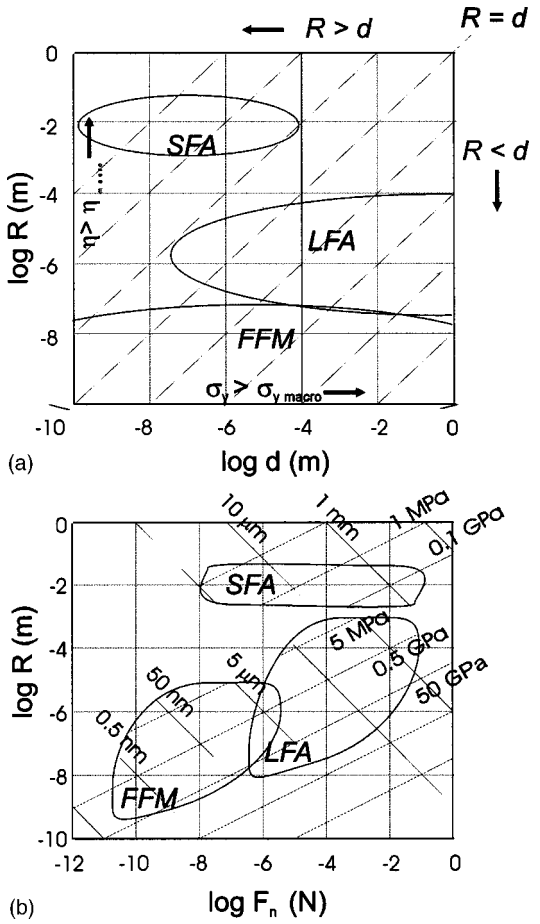

FIG. 4. Comparison of the working range of single asperity sliding friction apparatuses: LFA, FFM, and SFA. (a) Geometry of the contacts. Asperity radius R vs film thickness d. Areas of working range where physical size effects can occur have been indicated. For extremely thin viscous films the viscosity may increase above bulk values. For very small loaded contacts on metals the yield stress may increase above bulk values. Lines of constant R/d have been indicated. (b) Loading of the contacts. Lines of constant pressure and contact area two orders of magnitude apart are shown for Hertzian contacts. Numerical values are examples chosen to represent orders of magnitude found in the literature.

E. Single asperity sliding contacts

It has already been noted in Sec. II D that there is no such thing as *the* single asperity contact. The interpretation and even applicability of τ, in Eq. (6), depends on the contact situation. FFM and SFA do certainly not cover all relevant contact situations or even a continuous region in the experimental parameter space. In fact the LFA has been designed to study contact situations in a gap between the working ranges of FFM and SFA. It has been suggested that on many practical surfaces in sliding contact the asperities have radii in the order of a few microns, and that they carry loads of the order of mN. Contacts such as those lie within the working range of the LFA [Fig. 4(b)]. So the contact situation for a single asperity under normal load, depends on a range of parameters, and it may be expected that the situation in sliding friction shows similar complexities. These are not at all apparent in the friction ''laws'' that were introduced before.

And in fact, Eq. (6) has been used for contact situations for which the physical meaning of τ *must* differ.

Essentially elastic ''dry'' friction, without any damage to the surfaces involved and without any intermediate medium, is known as ''interfacial friction'' [25]. In interfacial friction, τ is thought of as a characteristic stress τ_c, or modulus, required to initiate *slip* along the interface

$$F_f = \tau_c A_{rz}. \tag{14}$$

In the interpretation of τ_c, analogies exist with the Peierls stress necessary for glide of dislocations or with crack propagation in solids. A number of detailed studies in interfacial friction have found that A_{rz} does indeed depend on F_n in a way predicted by contact mechanics, and that the dependence of F_f on F_n can entirely be attributed to that effect, but in other cases results seem to point to a form like Eq. (6) where in that case $\tau = \tau_c$.

In SFA experiments the geometry is essentially that of Couette flow: a film of thickness d is sheared between two identical interfaces [Fig. 4(a)]. In such geometries, for large enough d and assuming a no-slip condition at the interfaces, the behavior is expected to be governed by bulk material properties. This is essentially what rheometers are expected to show. One would expect slip to be constrained to the interfaces if $\tau_{c,\text{interface}} \ll \tau_{c,\text{bulk}}$, and to the bulk if $\tau_{c,\text{interface}} \gg \tau_{c,\text{bulk}}$. In the first case $\tau_{\text{eff}} \approx \tau_{c,\text{interface}}$ in the last case $\tau_{\text{eff}} \approx \tau_{c,\text{bulk}}$. The physical meaning of τ_{eff} *differs* from that of τ_c in interfacial friction because the exact plane where slip occurs is no longer specified and the value applies to a volume. For Newtonian fluids the shear stress depends linearly on the shear rate so $\tau_{\text{eff}} = \eta \tau_{c,\text{bulk}}(\dot{x}/d)$ with η a constant and $\tau_{\text{eff},\dot{x}/d=0} = 0$. If the intermediate material exhibits a yield stress at macroscopic scale a form like Eq. (6) might be expected. Also for very thin confined Newtonian films it appears that in fact $\tau_{c,\text{bulk}}(\dot{x}/d)_{\dot{x}/d=0} > 0$. Such a confined liquid will sustain elastic deformation, until at a certain point slip occurs, much as in a solid. In this particular case τ_{eff} is not expected *a priori* to be related to possible characteristic moduli of the bulk or the interfaces.

Bulk behavior can also be encountered in a single asperity contact that is deforming plastically. For metals it has been argued that, using Eq. (6) and Eq. (12)

$$F_f = \tau A_{rz} \approx \tau F_n / 3\sigma_0 \quad \text{or} \quad \mu \approx \tau / 3\sigma_0. \tag{15}$$

For many metals $\tau_{\text{bulk}} \approx \sigma_0/2$ so if one takes τ to be a treshold for *bulk* shear yield it follows that $\mu \approx 0.16$. Again the physical picture for τ is that of a certain volume of material with surface A_{rz} that is sheared for which $\tau_{\text{eff}} \approx \tau_{\text{bulk}}$.

In arriving at Eq. (15), the three-dimensional character of the contact is taken into account to calculate A_{rz}. However the slip, or dissipating process, is still supposed to be pure shear and the possible importance of the projected area A_{rx} is neglected. It is clear that A_{rx} must become important during sliding for increasing F_n and depth z. Even without adhesion between the asperity and the substrate, *repulsion* will cause substrate material to move sideways and to some extent downwards during sliding. This is called ''ploughing.'' For large enough z this material must deform in a way approaching that of the bulk substrate material. This will lead to a friction force and to dissipation. Ploughing is usually associated with plastic deformation but all deformation modes that limit the rate of deformation during sliding may be included.

Of course adhesion at the interface may change the deformation of the substrate during ploughing. The simplest possible way to incorporate both effects is to consider the repulsive (pure bulk) and adhesive contributions (interface and bulk via interface) to be completely independent. A modification of Eq. (6) to that effect was proposed by Bowden and Tabor [26]:

$$F_f = \tau_{\text{eff}} A_{rz} + \sigma_{\text{bulk}} A_{rx}. \tag{16}$$

In the following, Eq. (16) is taken as the friction ''law'' for the interpretation of our results, because the deformation during sliding usually involved bulk deformation in the sense indicated above, see Sec. III.

Now *steady sliding* is defined as the situation in which $\dot{x}(t) = v_s \wedge \ddot{x}(t) = \ddot{z}(t) = \dot{z}(t) = 0$. So during steady sliding there is equilibrium along $\hat{z}$, and $\sigma_z(t) A_{rz}(t) = F_n$, with $\sigma_z(t)$ the average stress exerted by the surface on the asperity, and $A_{rz}(t)$ the projection of $A_r(t)$ along $\hat{z}$. Anticipating Sec. III and Sec. IV, the following system of equations is proposed instead of Eq. (1):

$$\begin{aligned} m\ddot{x}(t) &= k_l[v_s t - x(t)] - F_f(t), \\ m\ddot{z}(t) &= \sigma_z(t) A_{rz}(t) - F_n. \end{aligned} \tag{17}$$

Equation (17) also includes situations for which $\ddot{x}(t) = \dot{x}(t) = 0$, in which case no sliding occurs.

III. EXPERIMENTAL SET UP AND RESULTS

A. Method

The LFA (Fig. 2) has been described in some detail elsewhere [3]. Here we will only mention the characteristics that are relevant for the experiments. The LFA probes and measures F_n and F_l independently. It uses two double leaf springs combined in a single leaf-spring unit as force probes and two focus-error detection heads to measure the deflection of the leaf springs. Normal spring constants are in the range 20–4000 N/m, lateral spring constants 7–1000 N/m. The optical heads combine a 10-nm sensitivity with a useful range of about 100 μm. The proven range of F_n is 400 nN–150 mN. During sliding F_n is kept constant by a feedbackloop using a piezotranslator that moves the leaf-spring unit along z. The range of driving speeds is, at this time, rather limited, from 1 to 40 μm/s. The leaf-spring units transduce friction and normal forces independently. Absolute values of normal and friction forces are calibrated and estimated to have typical errors less than 10%. The calibration is partly *in situ*, for the sensitivity of the optical heads, and partly *ex situ*, for the normal and lateral spring constants of the leaf-spring units. There is minimal coupling between the deflection measurements in lateral and normal direction. This coupling is also calibrated *in situ*. The response of the leaf-spring unit can effectively be approximated by a linear relation

$$\begin{pmatrix} \Delta z \\ \Delta x \end{pmatrix} = \begin{pmatrix} c_n & c_{nl} \\ c_{ln} & c_l \end{pmatrix} \begin{pmatrix} F_n \\ F_l \end{pmatrix}. \tag{18}$$

During the calibration of $c_{nl}, F_n = 0$ so $\Delta x = c_l F_l$ and $\Delta z = c_{nl} F_l = c_{nl} \Delta x / c_l$. For some units c_{nl}/c_l is as small as 0.003, a typical value is 0.01. This means that displacements of the tip normal to the surface can be measured with a reasonable error, if the absolute values are of the order $0.01\Delta x$ or larger. Consequently it can be concluded that the LFA is well suited for quantitative study of friction dynamics. The design of the leaf-spring unit allows for exchange of tips, that may be fabricated (e.g., etched) from wire material ($d \approx 0.4$ mm). The tips (or rather the asperities) used here are electrochemically etched tungsten wires. With a high-resolution (effectively about 5 nm) scanning electron microscopy (SEM) (XL30 FEG-ESEM) no protrusions were observed on the surface of these tips. Since the coatings used are soft and the penetration depths always greatly exceed 5 nm, we argue that the tips can be regarded as single asperities. The radius R of the tips is estimated from the SEM micrographs.

Coatings used consist of hexakis(methoxymethyl)melamine (HMMM) crosslinked polyesters, deposited with thickness of about 20 μm on Al substrates. Coatings with 10, 20, 30, and 40 wt % HMMM were investigated, in an attempt to qualitatively study the influence of material properties (changed via the crosslink density) on the sliding behavior [27]. A disadvantage of using thin film material is that there are no standard ways of measuring their rate dependent mechanical properties. Attempts to measure the mechanical properties were carried out with a nanoindentation apparatus, using standard interpretation schemes [28]. The results are treated as order of magnitude estimates only, considering the fact that no attempts were made to study the effect of deformation rate. In this sense the interpretation of the results has to remain qualitative.

All experiments were carried out under ambient conditions. Apart from the coating material, the following experimental conditions were varied in a systematic way: R, v_s, F_n, k_l. The influence of t_0 was not studied systematically. Some of the experiments were performed at sufficiently high sampling rate (10 kHz) to study the behavior during ''slip'' in detail.

B. Results and discussion

During the experiments interesting dynamic behavior was encountered. It shares a number of qualitative characteristics with multiasperity ''stick-slip'' systems that have been studied in terms of rate-and-state models. We find transitions from steady sliding to stick-slip for decreasing v_s and decreasing k_l, and increasing F_n but also transitions from steady sliding to stick-slip for decreasing tip radius R. All of these trends can be deduced from Fig. 5.

1. Transitions in sliding behavior

In Fig. 5 ''maps'' of dynamic behavior in dynamical parameter space, (v_s, F_n) in this case, show transitions from steady sliding to stick slip. Open circles indicate points in (v_s, F_n) space for which steady sliding was stable, closed circles indicate points where stick slip occurred. All three maps show a transition from steady sliding to stick slip for *decreasing* v_s and *increasing* F_n. A transition to stick slip for decreasing v_s is quite generally encountered in experiments described in literature (for reviews see, e.g., Refs. [7,11]). It is associated with ''velocity weakening,'' i.e., a decrease of F_f for increasing v_s. This was also observed here (not shown). The transition for increasing F_n has been observed in inertially loaded ($F_n = mg$) sliding multiasperity interfaces, for example, those described in Refs. [11], [12].

Comparison of the two maps in Figs. 5(b) and 5(c) with the map in Fig. 5(a) shows a shift of the transition to higher F_n for higher k_l. Again, this is a trend that has been found more generally. Comparison of the Figs. 5(b) and 5(c) shows the shift of the transition to F_n for increasing tip radius, R. Finally we find a transition to stick slip for a smaller amount of crosslinks [Fig. 5(d)].

2. Normal displacements

During steady sliding the asperity moves at some equilibrium depth z and ''ploughs'' through the surface. This depth was seen to increase with increasing F_n and decreasing v_s. At a certain combination of F_n and v_s steady sliding becomes unstable, and ''stick-slip'' motion occurs. From Fig. 6 it is clear that that mode of movement involves normal displacements of the asperity. The measurements shown correspond to the large closed circle at $(v_s, F_n) = (28\,\mu\text{m/s}, 7.2\text{ mN})$ in Fig. 5(a), so $k_l = 137$ N/m and $R = 4\,\mu$m. Monitoring the voltage applied to the piezo by the feedback loop in order to keep F_n constant, the movement of the tip normal to the surface can be observed during sliding. (To this end the piezo response was calibrated [3].) Furthermore, fast sampling (in this case 10 kHz) enables measurements during slip.

The absolute value of the penetration depth (up to a micron) is usually at least an order of magnitude larger than any roughness present on the surface of the tips. We argue therefore that the tips can be regarded as single asperities in these experiments. A considerable volume of material is being deformed during sliding and this deformation is assumed to be responsible for the largest part of the occurring dissipation.

Comparing Figs. 6(a) and 6(b) it is clear that during periods of increasing F_l, the asperity is deeper in the surface. In fact, during the increase of F_l, z increases and the asperity decelerates in x and z first and subsequently z decreases and the asperity accelerates in x and z. It is also clear that during slip, where F_l decreases rapidly, the asperity is at a relatively low depth z. A linear timescale such as used in Figs. 6(a) and 6(b) is quite inappropriate to present measurements at the widely different timescales apparent during this measurement, and a further clarifying graph is shown in Fig. 6(c). In that figure F_l has been plotted vs depth z. It can be observedthat the data for this regular stick-slip movement fall nicely onto a single limit cycle. The movement of the asperity during slip can now be clearly observed.

3. Steady sliding

The key to a physical understanding of dynamic friction behavior is to point out the mechanisms that tend to stabilize or destabilize steady sliding. The observation that unsteady movement is associated with normal movements evidently deserves consideration in this respect.

The experiments show that steady sliding is possible for a range of values of v_s, F_n, k_l, and R leading to specific values of F_f and z. During steady sliding, unlike in a static contact, material is constantly entering and leaving the contact. Some of this material is pushed aside and some of it is pushed down. The material resists this deformation with forces that exactly balance the forces exerted on it by the driving spring via the contact surface with the asperity.

The value of z will to a great extent determine A_{rz} and A_{rx}, which in view of Eq. (16) shows the importance of the z position for F_f. Of course A_{rz}, and therefore z, is important for the equilibrium along $\hat{z}$ as well, as was anticipated in Eq. (17). During steady sliding there is equilibrium along $\hat{z}$, so $F_n=\sigma_z A_{rz}$ with σ_z the average normal stress exerted on the asperity by the material as it is deformed along $\hat{z}$. Remembering the reasonable assumption that some of the material is pushed *down*, and passes underneath the asperity, it follows that movement along $\hat{x}$ of the asperity and deformation along $\hat{z}$ of the substrate are coupled.

Steady sliding at increasing asperity speed or depth will necessitate deformation at higher rates. Generally speaking materials, e.g., pseudoplastic or viscoelastic materials, resist higher deformation rates with higher pressures, which means that higher speeds $\dot{x}$ lead to increased upward pressure σ_z exerted by the material on the asperity. At constant F_n a new equilibrium can therefore only be reached if A_{rz} decreases, which means that the rigid asperity must move up. In other words $\sigma_z A_{rz}$ contains a *coupling* term $\sigma_{xz}A_{rz}$ that depends via σ_{xz} on v_s, or more generally on $\dot{x}$ of the asperity. For the resulting restoring normal force exterted by the substrate on the tip one can write $A_{rz}\sigma_z=A_{rz}(\sigma_{xz}+\sigma_{zz})$.

Clearly, this coupling term $\sigma_{xz}A_{rz}$ may be destabilizing and can potentially lead to ''velocity weakening,'' that is $\partial F_f/\partial v_s<0$. Higher deformation rates lead to *higher* stresses but also to *smaller* projected surfaces A_{rz} and A_{rx}. Whether $\partial(\tau_{\mathrm{eff}}A_{rz}+\sigma_{\mathrm{bulk}}A_{rx})/\partial v_s$ in which products of these terms ap-

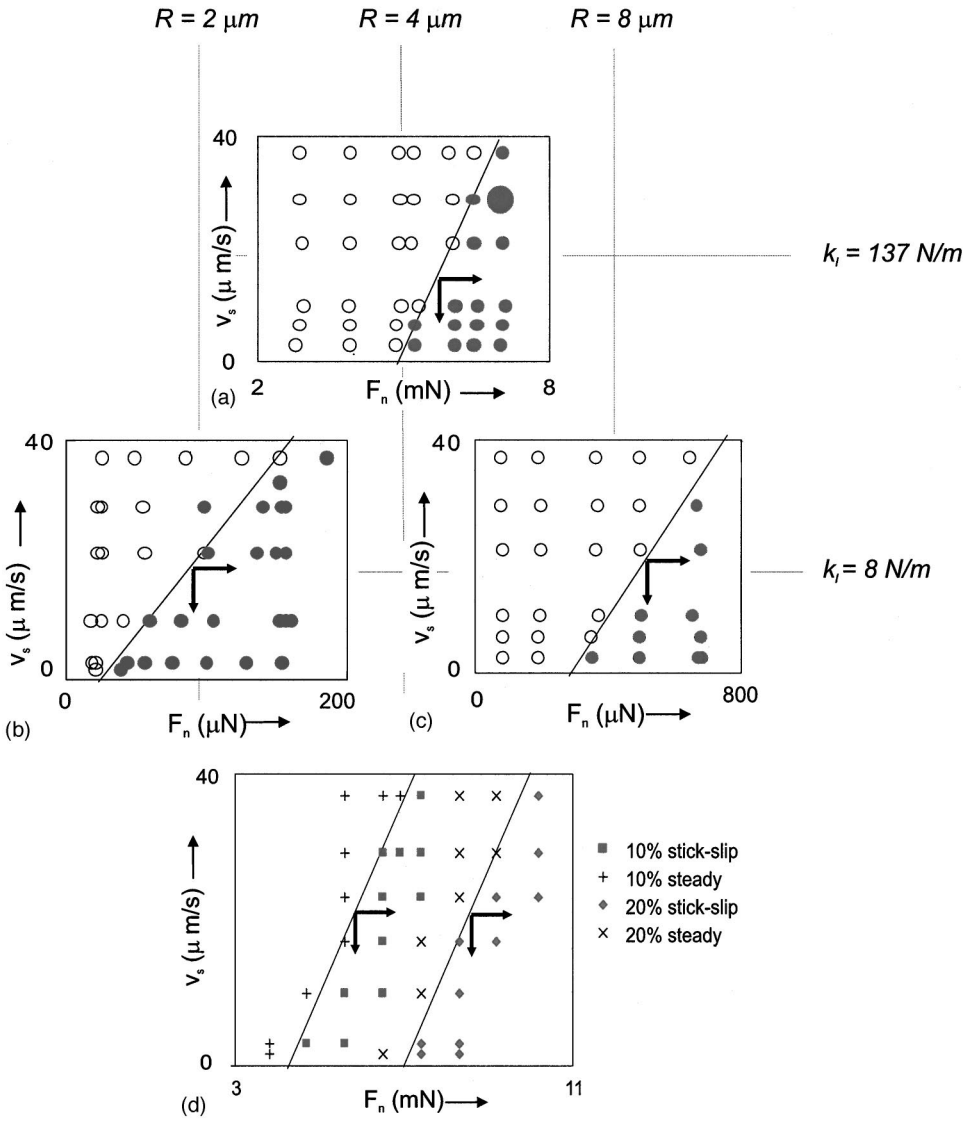

FIG. 5. ''Maps'' of dynamical $\{v_s, F_n\}$ phase space showing transitions in dynamic friction behavior. Closed circles represent points where stick-slip behavior occurred, open circles indicate steady sliding. Lines separating areas with these behaviors have been drawn as guides to the eye. Arrows indicate transitions from steady sliding to stick slip (a)–(c). Influence of asperity radius R and driving spring stiffness k_l on the transition. (d) Influence of crosslink density on the transition. Time-resolved measurements of the stick-slip trace indicated with a large symbol in Fig. 5(a) are presented in Fig. 6.

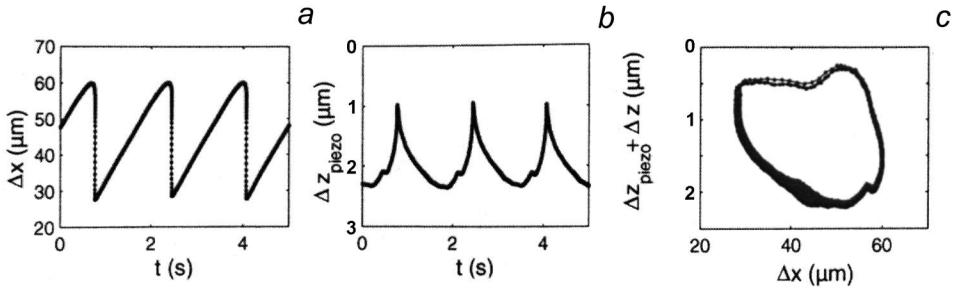

FIG. 6. Time-resolved (10 kHz) LFA measurement of stick slip, with $F_n=7.2$ mN, $v_s=28\ \mu$m/s, $k_l=137$ N/m, $R=4\ \mu$m, $c_{nl}/c_l=0.004$, and $c_n/c_n=0.0025$. This measurement is indicated with a large symbol in Fig. 5(a). (a) Deflection of driving spring vs time. (b) Extension of piezo element vs time. (c) z movement of asperity vs deflection of driving spring. During slip the feedback loop is not capable of reacting fast enough, which caused an increase of F_n with about 6%. As the piezo extension does not fully determine the z movement of the asperity in this case, the reading z_{piezo} is corrected by adding the simultaneously measured change in deflection z of the normal force leaf springs [3].

pear, is positive or negative, as a result of this is not *a priori* clear ''velocity weakening'' as well as ''velocity strengthening'' are possible as a result of an interplay between geometry and material behavior.

This particular coupling during sliding is usually not explicitly studied in experiment or considered in theoretical treatments. Tolstoi, in an early paper, was the first to point it out, based on experimental evidence [29]. He suggested that the influence of z displacements on A_{rx} may be crucial. More recently experimental evidence for x-z coupling has been found in sliding on granular substrates [8–10], boundary lubrication [15], and also in systems very similar to the one studied in this paper [30].

4. Stick slip

Let's assume that during steady sliding F_n increases. A new dynamic equilibrium may be reached at higher F_f and z, but for large enough F_n, such an equilibrium apparently does not exist. Without trying to explain why there is no new equilibrium it is still possible to understand which phenomena drive the motion of the asperity in this regime.

Whenever the asperity moves down, the upward force $A_{rz}(\sigma_{xz}+\sigma_{zz})$ exerted on it by the material is too small to balance F_n. Two effects limit the normal travel: the increase in A_{rz} and the increase in F_l caused by the driving spring. The latter will tend to increase the forward speed of the asperity, which in turn will lead to an increase in σ_{xz}. At a certain point F_n will be balanced and the continuous increase in F_l and σ_{xz} causes the asperity to start moving upward. Now, A_{rx} and A_{rz} are decreasing, which means that $\dot{x}$ may increase even more, and lead to even higher σ_{xz} and so on. Two effects will eventually limit this runaway behavior: the increase in normal pressure F_n/A_{rz}, and the decrease in F_l after the asperity has reached speeds higher than v_s.

So, starting from the requirements of the dynamic equilibrium during steady sliding and noticing the central role of the normal displacements, one arrives at a picture that involves a simple combination of asperity geometry and material behavior and gives a physically reasonable mechanism for the observed stick-slip behavior. Next, a description of this mechanism in a simple dynamical system is proposed.

IV. REPRESENTATION OF THE EXPERIMENTS IN A DYNAMICAL SYSTEM

A. Dynamical system

The aim is to find a dynamical system that qualitatively describes the movement of the asperity in contact with the surface and reproduces the experimental record presented in Sec. III B. The analogies between Eq. (5) and rate-and-state formulations have already been briefly discussed, in Secs. I and IV. As was discussed in Sec. II, Eq. (16) is assumed to be a reasonable first-order approximation for F_f. Together with Eq. (17) and the considerations in the previous paragraph, regarding the coupling of normal and forward motion, one arrives at

$$m\ddot{x}(t)=-k_l[x(t)-v_s t]\tau_{\text{eff}}(t)A_{rz}(z)-\sigma_x(t)A_{rx}(z),$$

$$m\ddot{z}(t)=-[\sigma_{zz}(t)+\sigma_{xz}(t)]A_{rz}(z)+F_n. \tag{19}$$

A description of the material behavior using constitutive equations that represent a collective evolution of all microscopic degrees of freedom in the contact is justified. The material in the contact resists deformation in a way that is typical for some volume rather than for an interface. So for τ_{eff} and σ_x a form is sought that relates them to averaged values of strain and strain rates in the substrate material in the contact.

Clearly the deformation of the contact may involve high strains and strain rates, and mixed stress states. The material response under these circumstances may be rather complicated. A range of nonlinear effects may be expected. At this stage we choose to simplify as much as possible and stay close to the rate-and-state formulations. From those we infer that a formulation in which the stresses are functions of strain rates only may already be rather successful. Introducing $\dot{\varepsilon}_x$ and $\dot{\varepsilon}_z$ for deformation rates associated with forward and normal movement, respectively, we write

$$m\ddot{x}(t)=-k_l[x(t)-v_s t]\text{-}\tau(\dot{\varepsilon}_x)A_{rz}(z)-\sigma_x(\dot{\varepsilon}_x)A_{rx}(z),$$

$$m\ddot{z}(t)=-[\sigma_{zz}(\dot{\varepsilon}_z)+\sigma_{xz}(\dot{\varepsilon}_x)]A_{rz}(z)+F_n, \tag{20}$$

TABLE I. Values used in the numerical calculations. Only values that *differ* from the ones in this table are mentioned in the figure captions. Calibrated values for R, F_n, v_s, and k_l have been used. Values for σ_0 and E^* were derived from nanoindentation experiments [25], and have been treated as order of magnitude estimates. L, η, and c are free model parameters for which no experimental estimates are available.

c	L (m)	η (Pa s)	σ_0 (Pa)	m (kg)	E^* (Pa)	k_l (N m)	R (m)
1	1×10^{-6}	20×10^{6}	70×10^{6}	1×10^{-4}	4×10^{9}	137	4×10^{-6}

As an approximation of the deformation rates $\dot{\varepsilon}_x$ and $\dot{\varepsilon}_z$ again the simplest possibility is chosen:

$$\dot{\varepsilon}_x=\frac{\dot{x}}{L},\quad \dot{\varepsilon}_z=\frac{\dot{z}}{L}, \tag{21}$$

where L represents some average of the width and depth of the track during an experiment. In rate-and-state models a similar characteristic length, called ''memory length'' there, is usually present.

We note that, because of the widely different time scales present in the experiments, such a formulation may be expected to fail during ''slip.'' A reasonable definition for a Deborah number is $\mathrm{De}=\tau\dot{x}(t)/L(t)$, where τ is a time scale typical for the material, and $\dot{x}(t)$ is the speed at time t. $L(t)$ is a typical length scale at time t, for example the average depth of the contact. $\dot{x}(t)/L(t)$ will be small during slow motion of the order of 0.01τ, large during swift motion, as much as 10000τ. In the calculations performed τ was typically of the order 0.1–1 s. This means that De changed from 0.001 to 1000. Assuming the material is viscoelastic it is probably safe to say that during the slow motion any elastic effects and details of the flow can be disregarded. However, this is clearly not the case during slip. We assume that the estimate of the elastic modulus E^* derived from the nanoindentation experiments (for $\dot{\varepsilon}\approx0$) is a reasonable order of magnitude estimate at much higher rates. This instantaneous modulus E^* means effectively that there is a minimum depth associated with sliding. As an estimate of this depth we take the depth z_0 at which the ''yield stress'' σ_0 would be reached in an indentation experiment [Eq. (14)]. Another reason for the occurrence of a minimum contact area, that might be represented by a minimum depth, can be pointed out. Adhesion between asperity and surface will lead to a finite contact surface for $z=0$ on retraction. Potentially, the fact that material piling up in front of the asperity may lead to a minimum sliding depth, it will definitely tend to reduce the upward force.

For the estimation of $A_{rz}(z,t)$ and $A_{rx}(z,t)$ it is assumed that the material in front of and on the side of the tip does not move upwards. The effect of adhesion on the contact area is neglected. For a reasonable estimate of the work of adhesion of $w=50\,\mathrm{mJ\,m^2}$ a radius of 10 μm and F_n of 1 mN, the ratio between the adhesive force and the normal force is about 0.001, which makes this a reasonable assumption. The tip is assumed to be effectively rigid. Considering the estimated values of yield stress and reduced modulus of the layers compared to those of tungsten that is also reasonable. These assumptions enable a straightforward calculation of first-order estimates of $A_{rn}(z,t)$ and $A_{rx}(z,t)$. For a paraboloid $\beta x^n=z$ with $n=2$ and $\beta=1/2R$

$$A_{rz}(z)=2\pi Rz,\quad A_{rx}(z)=\frac{4\sqrt{2R}}{3}z^{3/2}. \tag{22}$$

Finally an approximate functional representation of the material behavior has to be chosen. First we assume a material behavior approaching that of a Bingham viscoplastic medium:

$$\sigma(\dot{\varepsilon})=\sigma_0+\eta\dot{\varepsilon},\ \text{thus}\ \ \sigma_x(\dot{\varepsilon}_x)=\sigma_0+\eta\dot{\varepsilon}_x\ \text{and}$$

$$\sigma_z(\dot{\varepsilon}_z,\dot{\varepsilon}_x)=\sigma_0+\eta(\dot{\varepsilon}_z+\dot{\varepsilon}_x). \tag{23}$$

This form is used in the linear stability analysis. In the numerical calculations of actual dynamic behavior Sec. IV B3, $\sigma_x(\dot{\varepsilon}_x)$ is represented by

$$\sigma_x(\dot{\varepsilon}_x)=2/\pi\sigma_0\arctan[c_\sigma\eta\dot{\varepsilon}_x]+\eta\dot{\varepsilon}_x. \tag{24}$$

In practice we use $c_\sigma\geqslant10^5$, which means that the stress is of the order of the yield stress for $c_\sigma\eta(\dot{x}/L)\gtrsim\pi/2$, that means for $\dot{x}\gtrsim L\pi/2\eta c_\sigma$ or $\dot{x}\gtrsim10^{-5}\,\mu$ m/s. On the time scale of the experiment, this behavior is indistinguishable from Bingham behavior. This formulation avoids potential numerical problems when $\dot{x}=0$, where $\sigma(\dot{\varepsilon})$ should be equal to zero, and not to σ_0. Alternative formulations for the low strain rate behavior could lead to qualitative differences in the behavior at very low driving speeds, see Sec. V. The positive x direction is taken along the sliding direction; the positive z direction points into the material (see Fig. 1).

Introducing $x-v_st=x_1$; $\dot{x}-v_s=x_2$; $z=x_3$; $\dot{z}=x_4$; $z_0=x_{3,0}$, one finds the following dynamical system:

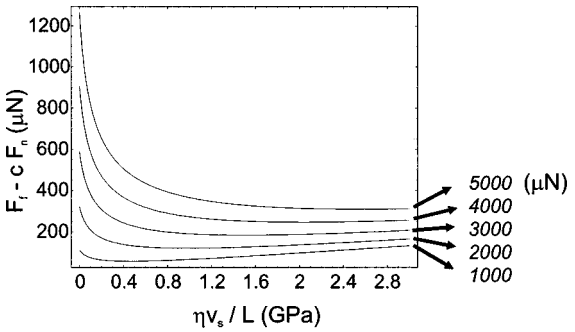

FIG. 7. Calculated friction force $F_f(v_s)$ during steady sliding using Eq. (28) for several values of F_n (indicated). Note velocity weakening at low v_s and transition to velocity strengthening.

$$\dot{x}_1 = x_2,$$

$$m\dot{x}_2 = -k_l x_1 - \frac{4}{3}\sqrt{2R}\left(\sigma_0 + \frac{\eta}{L}(x_2 + v_s)\right)x_3^{3/2} - 2\pi R\,\tau_{\text{eff}} x_3, \tag{25}$$

$$\dot{x}_3 = x_4,$$

$$m\dot{x}_4 = -2\pi R\left(\sigma_0 + \frac{\eta}{L}x_4\right)x_3 - 2\pi R\left(\frac{\eta}{L}(x_2 + v_s)\right)x_3 + 2\pi R\left(\frac{\eta}{L}(x_2 + v_s)\right)x_{3,0} + F_n.$$

This set of equations may be adapted to the type of loading: inertial, simple loading spring, or such as here with a spring in a feedback loop. In this particular case the inertial force $m\dot{x}_4$ is covered by the piezo, so, taking this term zero, Eq. (25) reduces to

$$\dot{x}_1 = x_2,$$

$$m\dot{x}_2 = -k_l x_1 - \frac{4\sqrt{2R}}{3}\left(\sigma_0 + \frac{\eta}{L}(x_2 + v_s)\right)x_3^{3/2} - 2\pi R\,\tau_{\text{eff}} x_3, \tag{26}$$

$$\dot{x}_3 = -(x_2 + v_s)\left(1 - \frac{x_{3,0}}{x_3}\right) + \frac{L}{\eta}\left(\frac{F_n}{2\pi R x_3} - \sigma_0\right).$$

B. Numerical results

Calculations were carried out to learn to what extent the description in Eq. (26) is able to reproduce the experimental record. Of importance are steady sliding behavior and its stability, their dependence on the dynamic parameters, and the shape of the limit cycle. Unless explicitly indicated, the values in Table I were used in the calculations presented.

1. Critical point or steady sliding

Steady sliding occurs in the critical point $\dot{x}_1 = \dot{x}_2 = \dot{x}_3 = 0$ in Eq. (26). [Steady sliding behavior is identical in Eqs. (25) and (26)]. One finds

$$x_3^c = \frac{1}{\sigma_0 + \eta\nu_s/L}\left(\frac{F_n}{2\pi R} + x_{3,0}\frac{\eta\nu_s}{L}\right)$$

and

$$F_f(\nu_s) = -k_l x_1^c = \frac{4}{3}\sqrt{2R}\frac{(F_n/2\pi R + x_{3,0}\eta\nu_s/L)^{3/2}}{\sqrt{\sigma_0 + \eta\nu_s/L}} + \tau_{\text{eff}}\left(\frac{F_n}{\sigma_0 + \eta\nu_s/L} + \frac{2\pi R x_{3,0}\eta\nu_s}{L(\sigma_0 + \eta\nu_s/L)}\right). \tag{27}$$

We see that $F_f(\nu_s)$ depends on R, $\eta\nu_s/L$, F_n, c, σ_0, E^*, and thus, in principle at least, it could describe the experimentally observed trends. Interestingly, taking $\tau_{\text{eff}}(\dot{\varepsilon}_x) = c\sigma(\dot{\varepsilon}_x)$,

$$F_f(\nu_s) = -k_l x_1^c = \frac{4}{3}\sqrt{2R}\frac{(F_n/2\pi R + x_{3,0}\eta\nu_s/L)^{3/2}}{\sqrt{\sigma_0 + \eta\nu_s/L}} + c\left(F_n + \frac{2\pi R x_{3,0}\eta\nu_s}{L}\right). \tag{28}$$

The *shear* term in Eq. (27) gives rise to a *Coulomb* term cF_n in Eq. (27). Figure 7 shows calculations of $F_f(\nu_s)$ using Eq. (28). For high speeds F_f behaves as $(4/3\sqrt{2R} + c2\pi R)x_{3,0}(\eta\nu_s/L)$. So we find ''velocity strengthening'' that depends on R, η/L, σ_0, and E^*. Depending on the values of the dynamic parameters a ''velocity weakening'' regime with $\partial F_f/\partial\nu_s < 0$ is possible for low speeds. From the partial derivative

$$\frac{\partial F_f}{\partial \nu_s} = \frac{2c\pi R\,\eta x_{3,0}}{L} + \frac{2\sqrt{2R}\,\eta x_{3,0}}{L}\left(\frac{F_n/2\pi R + \eta\nu_s x_{3,0}/L}{\eta\nu_s/L + \sigma_0}\right)^{1/2} - \frac{2\sqrt{2R}\,\eta}{3L}\left(\frac{F_n/2\pi R + \eta\nu_s x_{3,0}/L}{\eta\nu_s/L + \sigma_0}\right)^{3/2} \tag{29}$$

it is also clear this velocity weakening regime is possible because of the negative right-hand third term that can outweigh the other two. For values of ν_s for which $\partial F_f/\partial\nu_s > 0$, only steady sliding is stable, regardless of the value of k_l.

2. Linear stability of steady sliding

It is not *a priori* clear that steady sliding in the velocity weakening regime is unstable for a given spring stiffness k_l. Linear stability analysis of the critical point associated with steady sliding can resolve that matter. We have used the expression in Eq. (23) for $\sigma_x(\dot{\varepsilon}_x)$ in the linear stability analysis. The Jacobi matrix of Eq. (26) in the critical point is then

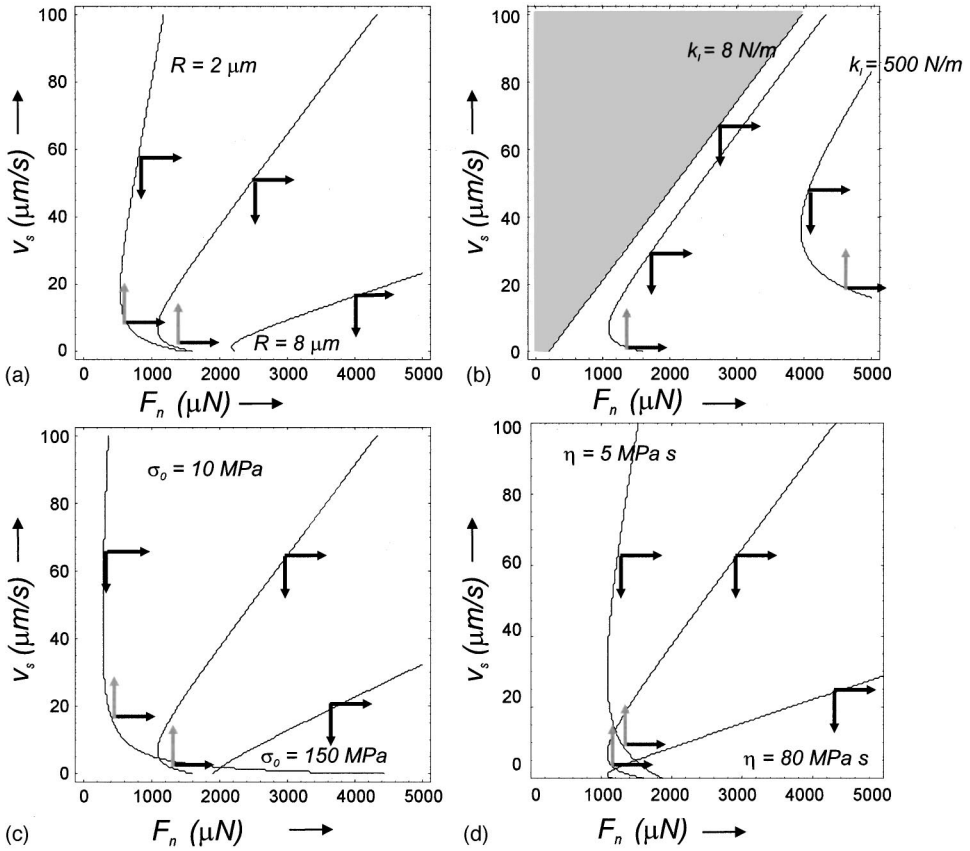

FIG. 8. Calculated maps of behavior in dynamical phase space. Parameters mentioned in Table I were used as basis. The curve calculated with these values returns in all four figures. Values indicated near a curve were the only ones changed with respect to Table I for that specific curve. Arrows point toward parts of phase space where steady sliding is unstable. Black arrows indicate behavior encountered in the experiments, gray arrows indicate behavior not encountered in the experiments (a) Influence of R. (b) Influence of k_l. Gray area: area for which $\partial F_f/\partial v_s>0$. In this area steady sliding is stable regardless of the value of k_l. (c) Influence of yield stress σ_0. (d) Influence of viscosity η.

$$[J]=\begin{pmatrix} 0 & 1 & 0 \\ \dfrac{-k_l}{m} & \left(-\dfrac{2c\,\eta\pi R x_3^c}{Lm}-\dfrac{4\sqrt{2R}\,\eta x_3^{c\,3/2}}{3Lm}\right) & \left(\dfrac{-2c\,\pi R(\eta\nu_s/L+\sigma_0)-2\sqrt{2R}\sqrt{x_3^c}(\eta\nu_s/L+\sigma_0)}{m}\right) \\ 0 & \dfrac{x_{3,0}}{x_3^c}-1 & -\dfrac{LF_m}{2\pi R\,\eta x_3^{c_2}}-\dfrac{\nu_s x_{3,0}}{x_3^{c_2}} \end{pmatrix}, \tag{30}$$

where x_3^c and $x_{3,0}$ are given by Eqs. (27) and (13), respectively. The linear stability in the critical point can be investigated by calculating the eigenvalues λ_i of [J], solving for the zeros of the characteristic polynomial: $\lambda_i^3+A\lambda_i^2+B\lambda_i+C=0$. A, B, and C are functions of all control variables that influence the transition in the experiments, R, F_n, ν_s, and k_l. Furthermore they depend on E^*,m,σ_0,η, that are accessible to experiment. This means a critical comparison of this model with the experiments is possible.

Analytic linear stability analysis leads to decidedly awkward terms, and the system is more easily studied by solving for the eigenvalues of [J] in Eq. (31) numerically. We have substituted the numerical values from Table I for all but one of L, η, R, m, σ_0, and k_l, and studied the behavior in the $\{F_n,\nu_s\}$ plane as a function of the value of the remaining parameter. Results, comparable to the experiment shown in Figs. 5(a)–5(d), are presented in Figs. 8(a)–8(d). Lines separate areas where $\mathrm{Re}[\lambda_i]<0$ for all λ_i from those where $\mathrm{Re}[\lambda_i]>0$ for at least one λ_i. The arrows across lines in the figure point to areas where $\mathrm{Re}[\lambda_i]>0$ for all λ_i, and steady sliding is not a stable solution. The precise character of the unstable motion in the other areas cannot be investigated in this way and requires separate calculations, see Sec. IV B3.

Concentrating first on that part of the Fig. 8(a) for which $\nu_s>10\,\mu$m/s, three of the characteristics mentioned in Sec. III B, transition from stable to unstable behavior for increasing F_n, decreasing ν_s, and decreasing R, are reproduced. Also the decrease in slope of the line separating stable and unstable areas for increasing R is in accordance with the experiments.

For low ν_s a deviation from this behavior is evident, indicated by the gray arrows, where steady sliding becomes a stable solution on *decreasing* ν_s. Such behavior was not apparent in our experiment, and will be discussed further on.

Figure 8(b) shows the effect of changing k_l. It can be seen that increasing k_l stabilizes steady sliding for all ν_s and F_n, a fact that is also evident from the experiments. The line for $k_l=137$ N/m is the same as in Fig. 8(a). A transition from

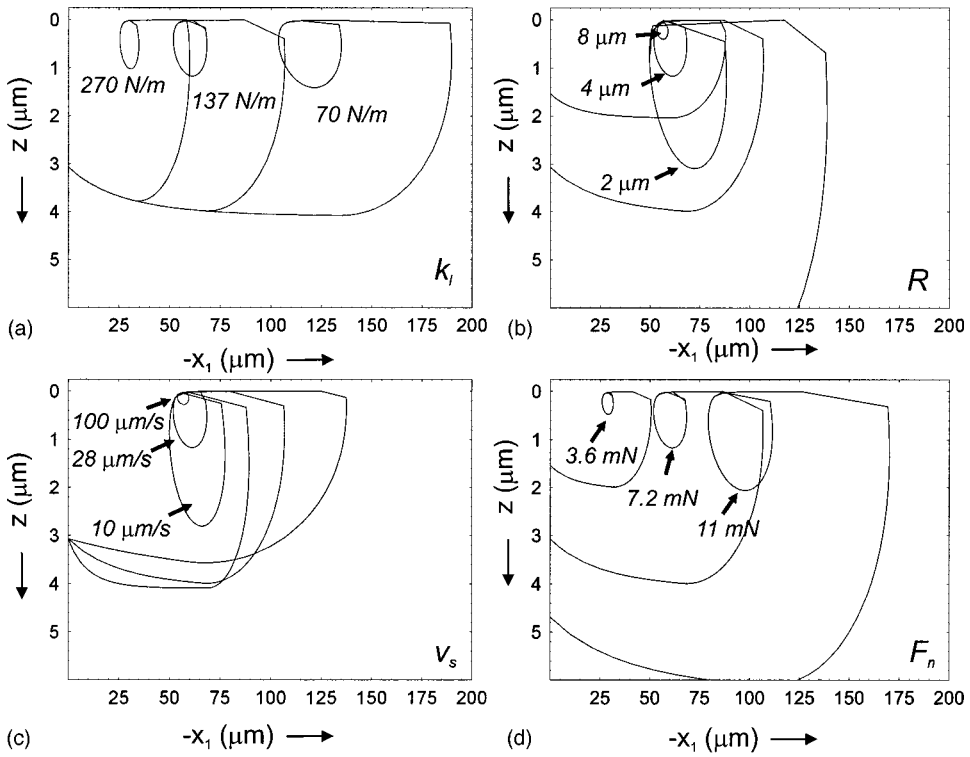

FIG. 9. Calculated $\{x_l, z\}$ phase portraits of stick-slip movements, using the dynamical system in Eq. (26), showing the influence of (a) k_l, (b) R, (c) v_s and (d) F_n.

stable to unstable behavior for increasing F_n and *decreasing* ν_s is again found for high ν_s. However it is interesting to see that the line for $k_l = 8$ N/m does not show this transition to steady sliding for decreasing ν_s at low ν_s. Apparently this low-velocity behavior depends sensitively on k_l being more apparent at high k_l. The line for 8 N/m almost coincides with the solution of $\partial F_f / \partial \nu_s = 0$ for these dynamic parameters. This means that this value of the spring constant does hardly stabilize the system against stick slip. Lower values of k_l will not lead to significant further destabilization.

Figures 8(c) and 8(b) show the effect of varying the phenomenological material parameters η and σ_0. For constant η and increasing σ_0 the unstable region moves to higher F_n and lower ν_s Fig. 8(c). For low σ_0 a region is again apparent where unstable motion stabilizes for decreasing ν_s. Interestingly there is also a region where steady sliding becomes stable for *decreasing* σ_0.

Keeping σ_0 constant and increasing η one finds that the region of unsteady sliding moves to higher F_n and lower ν_s. Fig. 8(d). Again a region is apparent where unstable motion stabilizes for decreasing ν_s, and similar as in the case of σ_0, there is also a region where steady sliding becomes stable for *decreasing* η. Only limited comparison with the experiment is possible at this stage. Assuming that an increase in cross-link density leads to an increase in both η and σ_0, calculations and experiments can be qualitatively reconciled.

All trends in the measurements are captured qualitatively by the calculations. However, as discussed above, the calculations show certain qualitative characteristics that have not been found in experiment. More extensive excursions in parameter space, especially toward lower speed, are needed in order to assess whether the trends predicted by the description do actually occur.

3. Dynamic behavior and limit cycles

The question remains whether any nonsteady movement resulting from solving Eq. (26) resembles the actual stick-slip movement found in the experiments [Fig. (6)], and whether transitory effects (sketched in Fig. 3) are captured. To investigate this, Eq. (26) has been solved [31] for several sets of dynamical parameters. The results are shown in Figs. 9(a)–9(d). Figure 9(a) shows phase portraits and limit cycles in $\{z, x_1\}$ space. These can be compared to Fig. (6). As a basis in the figures the behavior for $F_n = 7200\,\mu$N and $\nu_s = 28\,\mu$m/s has been taken, which is a stick-slip type movement. Figure 10 shows a number of graphs of F_l vs t.

A general characteristic of the limit cycles that is also apparent in the experimental results is the asymmetry during slow movement, or stick, in which there is always more forward motion during the downward movement than during the upward movement.

The other general trend that is recognizable, that for dynamic parameters closer to the stable subset the friction force and the stick-slip amplitude decrease, which was also found in experiment (not shown).

V. DISCUSSION AND CONCLUSIONS

The experimental record is qualitatively reproduced by the simple model presented, showing the influence of a number of dynamic parameters, R, F_n, ν_s, and k_l, and material properties represented by η and σ_0. This is interesting and slightly surprising considering the simplicity of the model in the treatment of stress states and material behavior. This constitutes a relevant point of discussion.

In this respect we would like to point out again the similarity between the description in Eq. (26) and the rate-and-

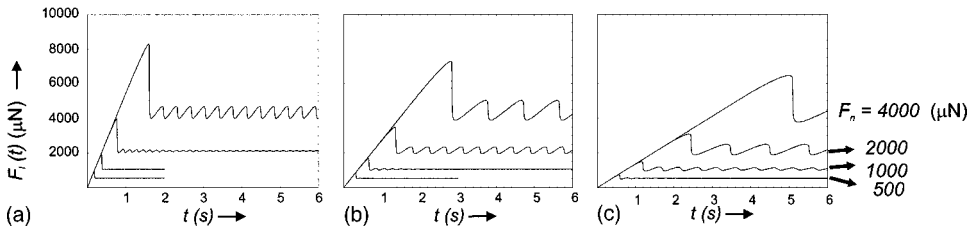

FIG. 10. Calculations F_l vs t using the dynamical system in Eq. (26), for various combinations of v_s (a) 40 μm/s, (b) 20 μm/s. (c) 10 μm/s), and F_l indicated to the right of (d) Other numerical values in accordance with Table I. The stick-slip traces show the characteristic form evident in the experiment (e.g., Fig. 6). Transitions from steady sliding to stick-slip behavior can be observed, and are in agreement with the linear stability calculations shown in Fig. 8.

state models with the general form of Eq. (4). These models are known to describe transitions from steady state to stick-slip sliding. A clear connection with the model proposed here and the rate-and-state models in the literature exists as is evident from the dynamical system in Eq. (25), that has a form equivalent to Eq. (4). Equation (25) is derived here from the dynamical system in Eq. (17), and alternative derivations, using more realistic assumptions on the behavior of the contact, may of course lead to different dynamical systems.

The key ingredient that leads to the coupling of the differential equations is in this case the x-z coupling by way of rate dependent material behavior. We would like to stress that x-z coupling is unique to the sliding contact and that the study of stationary contacts, is in this sense, of limited value for the understanding of sliding friction. Regarding z as a state parameter the equivalence of this description with the rate-and-state descriptions becomes clearer. In rate-and-state descriptions for ''dry'' friction, the state parameter is usually loosely related to A_{rz}. In this case an explicit relation to A_{rz} and A_{rx} is proposed using various simplifying assumptions. Sec. IV B, starting from the friction ''law'' in Eq. (16). The choice of friction law, Eq. (16), was motivated in Sec. III E, indicating that under the experimental conditions pressures underneath the asperity must lead to substantial irreversible deformation of some contact volume in the substrate.

Clearly, in all the descriptions of dynamic sliding behavior major assumptions are made and this case is not different in this respect. However, this is clear where assumptions were made and what they entail. This should aid further experimental and theoretical efforts. A few remarks on subsequent work are appropriate.

The chosen material behavior is characterized by a stress that increases monotonously with applied strain rates. The velocity weakening in the model is due to the normal motion, caused by the inability of the substrate material to respond in phase with the deformation at high rates applied, and the geometry of the asperity. This ground for weakening was originally proposed by Tolstoi [29]. A subtle difference with the rate-and-state models in the literature is that there the weakening behavior is often put *into* the dynamical system, rather than following it, as is the case here.

The velocity strengthening at high velocities is tentatively connected to a lower limit on the sliding depth and thus to the projected contact surfaces of the deformed volume. This limit on the sliding depth may be attributed to the instantaneous modulus of the substrate or, alternatively, on adhesion at the sliding interface or on pile up of the deforming substrate, effects that have not been explicitly entered in the description here.

The simplicity of the contact situation, and the detailed experimental record, were helpful in analyzing this specific single asperity sliding friction contact. Its relation with other single asperity contacts has been pointed out in Figs. 4(a)–4(c). Deliberately designing experiments so that parts of the working ranges overlap, would be helpful in mapping out possible qualitative changes in sliding behavior and whether they are in any way related to the different contact situations that may be defined for stationary contacts.

Concentrating on contact situations within the range of the LFA, the main question is whether the results presented here have any significance pertaining to more practical, and as some would argue more interesting, multiasperity situations.

Single asperity contacts can in some aspects be similar to multiasperity contacts. This should already be evident from the success of rate-and-state descriptions for multiasperity contacts as those do not refer to individual asperity contacts of the multiasperity contact. When enough contacts are present, sufficient averaging over the individual properties and behavior occurs and individual asperities are not apparent in the experimental record. The question is whether the averaged behavior is similar to the behavior of a single asperity contact. In this respect a notion introduced by Baumberger is interesting. He defines contacts that consists of enough asperities to allow for decent averaging, but that are ''dilute'' in the sense that during an experiment an individual asperity will be in sliding contact only one time, or not at all. This means that a true single pass experiment is taking place. Any irreversible changes to the asperities (on a time scale that would be characteristic for the time between two sliding events of an asperity) will not appear in the sliding behavior. One could further demand that all individual contacts in such a dilute multiasperity sliding contact are independent. Meaning that the behavior of one of the sliding contacts at some time would be indistinguishable from its behavior as a single asperity. In the case at hand is it likely that two asperities that are separated by a distance $\gg R$ will behave in such a way. In that case a situation arises that is very much like a single asperity contact. Judicious experimenting with situations that approach multiasperity contacts ever closer, starting, e.g., from two-asperity contacts with adjustable geom-

etry, or single asperity contacts on substrates with adjustable geometry might indicate whether any qualitative changes in behavior occur when the multiasperity contact situation changes from a set of noninteracting sliding asperities to a set of interacting sliding asperities. The linear stability analysis of the present dynamical system shows how complicated the nonlinear response of a sliding system may be to a change in relevant dynamic parameters. Clearly linear extrapolations of sliding friction behavior cannot be expected to be meaningful *a priori* and the experiments proposed should cover as wide a region of dynamical parameter space as possible.

In conclusion, the fact that a dynamical system that incorporates a simple friction law, combined with rough approximations of the resulting forces on the asperity, already leads to qualitative agreement with all measured trends, is rather hopeful. Notwithstanding this fact, the proposed model must be considered a first attempt. Considering the simplicity of the description with respect to material behavior and stress states, it seems clear where improvements are needed and it is reasonable to assume that they could lead to more quantitative agreement. It is believed this work may be useful as a guide to further experimental and theoretical work, adressing practical as well as more fundamental issues, especially in the area of friction and wear of polymers.

[1] C. M. Mate, G. M. McClelland, R. Erlandsson, and S. Chiang, Phys. Rev. Lett. **59**, 1942 (1989).

[2] J. Israelachvili and P. J. McGuiggan, J. Mater. Res. **5**, 2223 (1990).

[3] C. P. Hendriks and W. P. Vellinga, Rev. Sci. Instrum. **71**, 2391 (2000).

[4] J. H. Dieterich, J. Geophys. Res. **84**, 2161 (1979).

[5] A. Ruina, J. Geophys. Res. **88**, 10 359 (1983).

[6] For a recent review: C. Scholz, Nature (London) **391**, 37 (1998).

[7] H. Yoshizawa and J. N. Israelachvili, J. Phys. Chem. **97**, 11 300 (1993).

[8] S. Nasuno, A. Kudolli, J. P. Gollub, Phys. Rev. Lett. **79**, 949 (1997).

[9] J. C. Géminard, W. Losert, and J. P. Gollub, Phys. Rev. E **59**, 5881 (1999).

[10] W. Losert, J. C. Géminard, S. Nasuno, and J. P. Gollub, Phys. Rev. E **61**, 4060 (2000).

[11] T. Baumberger, Solid State Commun. **102**, 175 (1997).

[12] F. Heslot, T. Baumberger, B. Perrin, B. Caroli, and C. Caroli, Phys. Rev. E **49**, 4973 (1994).

[13] See, e.g., Jianping Gao, W. D. Luedtke, and Uzi Landman, Phys. Rev. Lett. **79**, 705 (1997) and references therein.

[14] J. Grasman, *Asymptotic Methods for Relaxation Oscillations and Applications*, Applied Mathematical Sciences Vol. 63 (Springer-Verlag, New York, 1987).

[15] A. Dhinojwala, S. C. Bae, S. Granick, Tribol Lett. **9**, 55 (2000).

[16] J. A. Greenwood and J. P. B. Williamson, Proc. R. Soc. London, Ser. A **259**, 300 (1966).

[17] I. N. Sneddon, Int. J. Eng. Sci. **3**, 47 (1965).

[18] K. L. Johnson, K. Kendall, and A. D. Roberts, Proc. R. Soc. London, Ser. A **324**, 301 (1971).

[19] B. V. Derjaguin, V. M. Muller, and Y. P. Toporov, J. Colloid Interface Sci. **53**, 314 (1975); M. F. Linker and J. H. Dieterich, J. Geophys. Res. **97**, 4923 (1992).

[20] D. Maugis, J. Colloid Interface Sci. **150**, 243 (1992).

[21] R. W. Carpick, D. F. Ogletree, and M. Salmeron, J. Colloid Interface Sci. **211**, 395 (1999).

[22] K. L. Johnson, in *Micro/Nanotribology and its Applications*, edited by B. Bhushan (Kluwer Academic, Dordrecht, 1997).

[23] For example, M. Giri, D. Borsfield, W. M. Unertl, Tribol. Lett. **9**, 33 (2000).

[24] K. L. Johnson, *Contact Mechanics* (Cambridge University, Cambridge, 1985).

[25] E. Kumacheva, Prog. Surf. Sci. **58**, 75 (1998).

[26] F. P. Bowden and D. Tabor, *The Friction and Lubrication of Solids* (Oxford, Clarendon, 1950).

[27] S. Frings, thesis, Eindhoven University of Technology, 1999.

[28] W. C. Oliver and G. M. Pharr, J. Mater. Res. **8**, 297 (1993).

[29] D. M. Tolstoi, Wear **10**, 199 (1967).

[30] K. Li, B. Y. Ni, and J. C. M. Li, J. Mater. Res. **11**, 1574 (1996).

[31] NDSolve, Mathematica 4.0, www.wolfram.com